

A deterministic model for forecasting long-term solar activity

Eleni Petrakou*

Athens, Greece
September 7, 2017

Abstract

The successive long-term increase and decrease in Sun's activity associated with solar cycles has not been connected to a definite underlying mechanism so far, hence predictions about its amplitude usually depend on extrapolation from the sunspot number of previous cycles or observations of the geomagnetic field, becoming available only very close to or after a cycle's start and often departing from the actual events. Here we present a phenomenological model for quantitative description of the cycles' characteristics in terms of the number of M and X-class solar flares. The main element of the model is the relative ecliptic longitude of the planets Jupiter and Saturn. Using as input the temporal distribution of flares during cycle 21, we obtain distributions for cycles 22-24 in notable agreement with the observed ones. Elements of shorter-term description can be elaborated further, however we are able to provide predictions for the evolution of solar activity for the rest of cycle 24 and for cycle 25. This deterministic description could contribute to elucidating the underlying physical mechanism and forecasting space weather.

Contents

Introduction	2
1 Observations and conventions	3
2 The model	5
2.1 Jupiter-Saturn approach and coupling to the 11-year modulation	5
2.2 Timing of the 11-year modulation	10
2.3 Overview	11
3 Forecasting cycles 24 and 25	12

*E-mail: helen@petrakou.net

4 Further discussion	13
4.1 Other planetary effects	13
4.2 Historical activity	14
4.3 On physical mechanisms	14
5 Conclusions	15
Bibliography	17
Appendices	18
A Performance and statistical testing	18
A.1 Performance	19
A.2 Timing	19
B Systematic uncertainties	21
B.1 Binning effects	21
B.2 Average cycle length	22

Introduction

Although the characteristic repetition in solar activity approximately every 11 years is apparently connected to the Sun’s magnetic field, no definite underlying mechanism has been established; predictions about the amplitude of solar cycles usually depend on extrapolation from the sunspot number of previous cycles[1] or indirectly on observations of the geomagnetic field[2], becoming available only very close to or after a cycle’s start[2, 3, 4] and often departing from the actual events. A comprehensive overview of solar cycle research and prediction methods can be found in [5]. Both short-term activity, e.g. solar storms, and its long-term evolution in cycles affect terrestrial events, including telecommunications and global climate.

Here we present a phenomenological model for the quantitative description of individual cycles’ features, such as start, intensity, evolution, in terms of the number of M and X-class solar flares. Recent work[6] reported correlation between the eruption of solar flares and the positions of the inner planets; here, relevant notions are extended with the

inclusion of the two gas giant planets, the use of relative instead of absolute positions, and the focus on long-term solar activity. The main factor of the model is the relative ecliptic longitude of the planets Jupiter and Saturn. Using as input the data of cycle 21 we are able to reconstruct satisfactorily the latest three cycles and provide predictions for the next years.

Section 1 describes the used observations and their treatment. Section 2 presents the details of the model, which comprises of two main components. Section 3 provides predictions for the rest of the current cycle and the next one. Section 4 discusses briefly further points (effects related to the other planets, past activity, and bibliography on possible underlying physical mechanisms). Conclusions are found in Section 5. In addition, Appendix A presents performance and statistical tests of the model, while Appendix B gives details about the sources of systematic effects and their derivation.

1 Observations and conventions

Solar flares

Sunspots are darker areas on the surface of Sun, corresponding to reduced local temperature, caused by concentrations of magnetic field flux; their typical lifetime is in the order of days. Solar flares occur from abrupt release of magnetic energy and are related to sunspots since they both occur in magnetically active regions of the photosphere; the emission from flares spans the whole electromagnetic spectrum and includes massive particles, with duration in the order of minutes. While studies of the solar cycle traditionally use the sunspots as observable, here solar flares will be employed: While sunspots are indirect indicators of underlying dynamics, flares are actual physical events with definite timing and released energy, as well as real impact on space weather. The obvious drawback is being constrained to examining the four latest cycles, for which solar flare records exist.

Solar flares are categorized on a logarithmic scale according to their X-ray brightness. The top three categories are known as C-class, M-class and X-class, in increasing order, with M-class spanning 10^{-5} - 10^{-4} W/m² and X-class including all higher values. At the present stage of this study only the solar flare counts are used without considering their intensity; this treats the occurrence of flares as statistical timed events. Typically, C-class activity occurs almost daily releasing small amounts of energy, therefore we restrict the sample to M-class and X-class flares, since their emergence involves less randomness. Intensities and all flare classes are planned to be examined at a next stage.

Since the start of cycle 21 up to the end of year 2016 there have been 6,339 and 491 M and X-class flares (Fig.1). The count for each cycle is quoted in Table 1. The data are X-ray flux measurements of the NOAA SMS and GOES satellites[7]. In order to have an exact overview of the effects under discussion no smoothing is applied on the distributions, other than the binning in histograms.

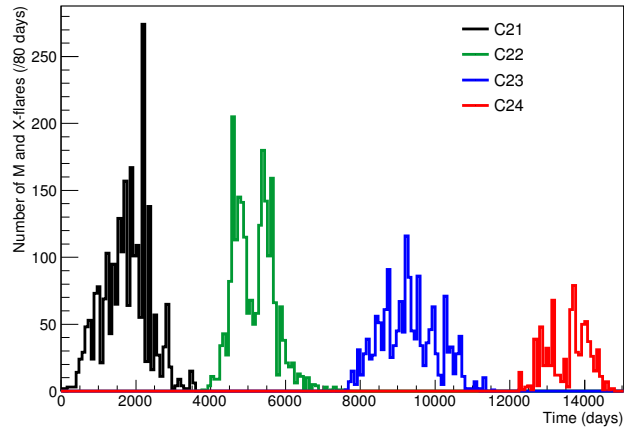


Figure 1: *Number of M and X-class flares as a function of time, for solar cycles 21-24. The range starts on 1977/01/31; the end of year 2016 is found at day 14,894. Each cycle is plotted in a different colour (see text for definition of start and end dates).*

Timing convention

We will define the start of each cycle by the appearance of the first flare erupting from a sunspot with reversed magnetic polarity (according to [8]). The end of each cycle is defined by the start of the next one. The resulting dates and durations are found in Table 1. For completeness it can be noted that, with this definition, thirteen flares of cycle 20 and one flare of cycle 22 occurred during the following cycle; these are not included in the analysis.

Table 1: *Number of flares, duration and start months of the four latest solar cycles (see text for definition of start and end dates).*

Solar cycle	Number of M and X-class flares	Start month	Duration (days)
21	2,175 / 163	Jan 1977	3,548
22	2,021 / 156	Oct 1986	3,817
23	1,434 / 127	Apr 1997	4,676
24	702 / 38 (ongoing)	Jan 2010	2,537 until end of 2016

Convention for the relative angle of the two planets

In the rest of the text, the relative heliocentric ecliptic longitude between Jupiter and Saturn will be used frequently. All quoted angles will refer to the two planets' relative ecliptic longitude, with either conjunction or opposition corresponding to zero degrees, i.e. both cases of alignment are treated equivalently.

For illustration, if Jupiter is found at 30° ahead of Saturn then the relative angle is $+30^\circ$ (Fig.2, case a), while if it is at 345° ahead of Saturn then the relative angle is -15° (Fig.2, b). If Jupiter is found at 160° ahead of Saturn then the relative angle will be -20° (Fig.2, c), since they are approaching their next closest alignment, which will be the next opposition. Consequently, the range of values of the relative angle is $[-90^\circ, 90^\circ]$. Note that, for instance, “ 91° ” is actually -89° , since the closest alignment is the next opposition.

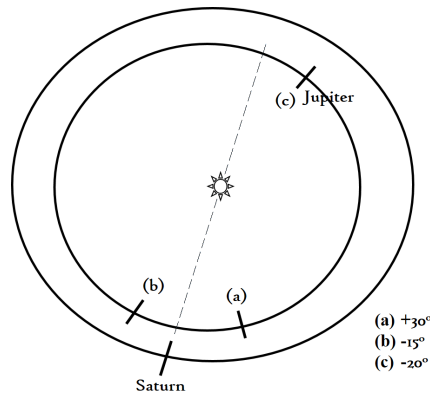


Figure 2: *Examples for the relative angle between the two planets according to the convention used in the text.*

2 The model

This study focusses on the general features of solar cycles -such as start, duration, intensity, overall development- in terms of the number of M and X-class flares (“flares”). We will demonstrate that such features can be described in a deterministic way by a model describing the synergy of two contributions. Paragraph 2.1 exposes the model and its descriptive role, while Paragraph 2.2 deals with its predictive role. A brief overview is given in Paragraph 2.3.

2.1 Jupiter-Saturn approach and coupling to the 11-year modulation

The principal component of the model is an apparent coupling between the empirical 11-year range commonly associated with solar cycles (“established” range) and the relative angle between Jupiter and Saturn (“the two planets”). This arises from the empirical observation that in each of the four latest cycles the solar activity appears “dragged along” around the two planets’ alignments, while getting weaker as the alignments occur progressively further from the temporal middles of the cycles (demonstrated in Fig.3).

More precisely, it is proposed that *the main drive behind the evolution of solar activity is strongly correlated to the relative ecliptic longitude of Jupiter and Saturn; however, this effect can only act within the constraints of the established 11-year range.*

In this Paragraph, these two contributions will be quantified by using two distributions extracted from the observations. Because of these quasi-periodic contributions' different lengths¹, their combined effect changes with time; their coupling will be quantified by displacing them appropriately and obtaining their common area. We will then demonstrate that the distribution of this overlap area can describe the global characteristics of the solar cycles to a satisfactory degree.

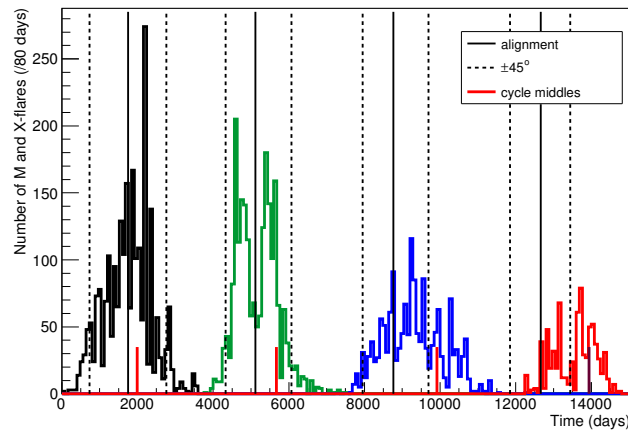


Figure 3: *Distribution of flares for the four latest cycles, with guides plotted at the temporal middle of each cycle and at -45° , 0° and $+45^\circ$ around the two planets' alignments. For the ongoing cycle, the temporal middle (purple) was placed at one average cycle length after the last measured middle.*

The Gaussian distributions

The quantification of the above proposition starts with certain assumptions:

- The effect of each of the two contributions on the solar activity follows a Gaussian distribution.
- Both contributions are equally strong, therefore the two distributions have the same maximum height².
- Empirically, the established range spans roughly 11 years. When the two planets'

¹The established contribution fluctuates around approximately 11.0 years. The Jupiter-Saturn synodic period oscillates around its average of ~ 19.9 years, with alignments found at half this length.

²Abandoning this assumption does not provide obviously improved results.

relative longitude is considered, then activity is observed to be stronger mostly within the range of -45° to $+45^\circ$ around their alignment (Fig.3).

Using these assumptions, two distributions will be extracted from the observations, one corresponding to the Jupiter-Saturn approach and one corresponding to the established “11-year” period. The assumptions can be translated into the following requirements about the Gaussian functions:

- One of the Gaussians is centered on the middle of the cycle, and the other is centered on the date of the Jupiter-Saturn alignment.
- Both functions have the same constant.
- Their $\pm 2\sigma$ ranges roughly cover, respectively, 3,000 days and between the dates of -45° to $+45^\circ$ around the alignment.

For their extraction we will use cycle 21 where, by a useful coincidence, the two planets’ conjunction took place only 238 days before the middle of the cycle: Therefore we will assume that in cycle 21 the deployment of both effects in their full ranges can be seen, and both distributions can be obtained from the data.

The temporal middle of cycle 21 was placed on zero and the axis expanded to $\mp -2,000$; the bin with 276 entries was considered an outlier and was arbitrarily halved. The means of the two Gaussian distributions were fixed on the corresponding dates, while the ranges for the constant and the standard deviation were constrained as described above. In this case minimization of the fitting function’s parameters is not the most suitable approach, as it will be driven by the intense small-scale fluctuations in the solar activity. What was preferred was to follow the envelope of the data within each of the two respective ranges. The two resulting functions are shown in Fig.4. Their parameters are given in Table 2. The ROOT[9] package was used for their extraction.

The individually plotted distribution of cycle 21 has short-scale differences with respect to Fig.1, due to the different start dates of data with respect to the start dates of the bins; systematic uncertainties resulting from the binning choices will be assigned to the model (shown later in Fig.6). Appendix B.1 gives details about their derivation.

Coupling

After obtaining the two distributions corresponding to the two considered effects, the next step is to center the “11-year” Gaussian distributions on the dates of *each cycle’s* temporal middle. The Jupiter-Saturn Gaussian distributions are centered on the subsequent dates of the two planets’ alignments. Provisionally, the middle of the ongoing cycle 24 is placed at the average sunspot length (4,015 days) after the measured middle of cycle 23 (see also Paragraph 2.2). It should be stressed that, for all cycles, the two distributions used are those obtained from cycle 21.

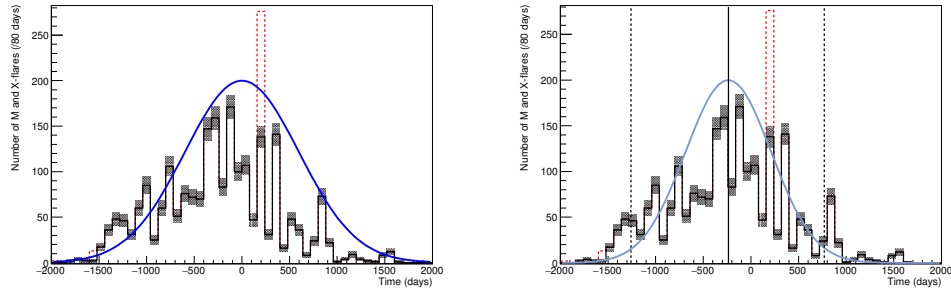


Figure 4: *Distribution of flare counts for cycle 21 and the Gaussian functions corresponding to the “11-year” effect (left) and to the Jupiter-Saturn effect (right). In the case of the Jupiter-Saturn effect, guides are plotted at -45° , 0° and $+45^\circ$. Poisson errors are shown on the data. The bin with the highest content was arbitrarily halved; a few flares close to the start of the cycle (dashed red) belong to cycle 20.*

Table 2: *Parameters of the two extracted Gaussian functions, for binning in 80 days. The Jupiter-Saturn mean refers to cycle 21.*

	constant	mean	st. deviation
“11-year” Gaussian	200	0	600
Jupiter-Saturn Gaussian	200	-238	450

As mentioned above, it is proposed that the area of overlap of the two Gaussians can describe the coupled effect of these two contributions. Accordingly, the two functions and their binned common areas are plotted in Fig.5, for the time range of the four cycles. *The latter distribution quantifies the two contributions and their coupling.*

Comparison to data

In Fig.6, the data are overlaid on the binned model distribution. The statistical uncertainty is the Poisson error on the predicted number of flares per bin. The systematic uncertainty comes from the binning effects (with the derivation discussed in Appendix B.1). For cycle 24 it also comes from the timing of the “11-year” Gaussian, as discussed in the next Paragraph (its derivation is found in Appendix B.2).

The model appears to be in noticeable agreement with the data on the timing, intensity and general evolution of activity in each cycle, and also roughly on the total span.

Angular range of activity

Although no physical mechanism is inferred yet, phenomenologically the solar activity seems to be regulated by the approach and retreat of the two gas giants, with conjunction and opposition having equal roles. Under the scheme presented here, when the two planets start approaching to their alignment closer than -90° , a build-up of activity begins

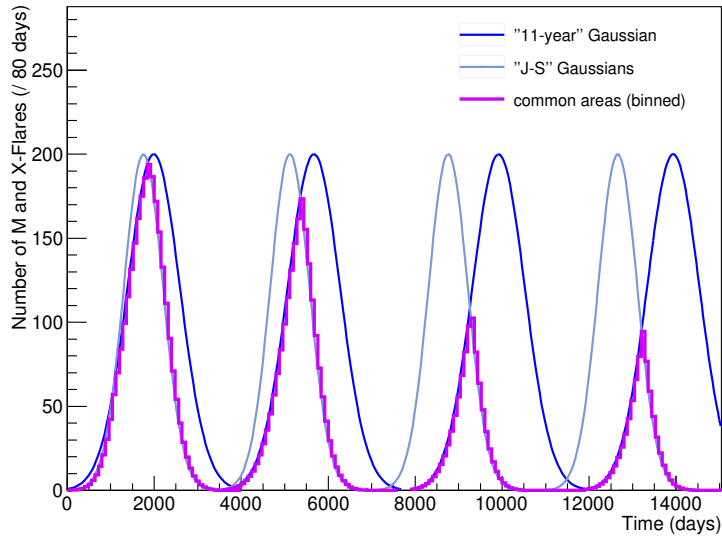


Figure 5: *The two types of Gaussians centered on the respective dates, and the binned distributions resulting from their overlap.*

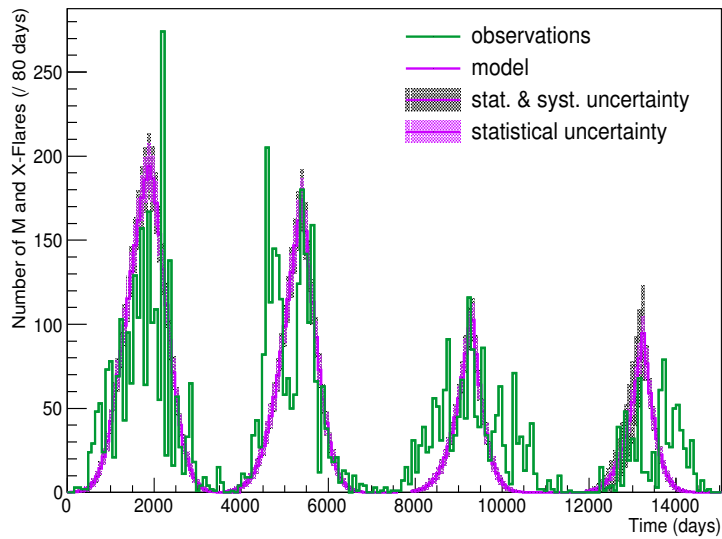


Figure 6: *Flare counts for the last four cycles (green), overlaid with the model distributions. The model includes statistical and systematic uncertainty. (The end of year 2016 is found at day 14,894.)*

and manifests after some further approach; when the planets move away from alignment the activity starts to decrease, following however the “bounds” of the established contribution. Finally, when they retreat further away than $+90^\circ$, the activity dies off as a new phase of approach to the next alignment actually begins.

A notable case of the last point seems to be the ongoing cycle. Several prediction methods, even updated as late as 2009, expected smoothly decreasing activity in 2016 and later[3]. In reality the solar activity almost disappeared after the retreat further than $+90^\circ$ in December 2015, with only a handful of M-class flares in 2016 and 32 spotless days.

Although the model agrees with the main part of the four cycles in the overall intensity and timing, time ranges outside the overlap are not described by it, particularly the two cycles with “double peaks”. Empirically however, the ranges where both Gaussians still have significant strength are seen to host activity of intensity comparable to the main part. This point is left to be quantified at a subsequent stage of the analysis.

2.2 Timing of the 11-year modulation

The model as presented so far is descriptive about the long-term evolution of activity, but not predictive since it requires knowledge of the date of each cycle’s middle, which was obtained from observations (Paragraph 2.1). However, if the “11-year” Gaussian distribution is centered on one average cycle length away from the latest measured cycle middle, the resulting modeling is close to that obtained in the first instance.

More precisely, the recorded average duration of the 23 sunspot cycles is 11.02 years (4,015 days), with a deviation of 10%. Using this length and the measured middle of cycle 23, the middle of cycle 24 falls on 7th April 2015; this date was used for centering the “11-year” Gaussian in the plots of the previous Paragraph. (It must be noted, however, that using as exact a number as 4,015 might be larger precision than should be used: The sample of documented cycles is rather small, their durations vary strongly, and the calculation is affected by determining the cycles’ starts from the sunspots’ field reversal instead of the onset of flares³.)

Fig.7 shows the predicted distribution as obtained in the previous Paragraph and as obtained by placing each cycle’s middle on the average number of days after the previous measured middle; as mentioned, the two resulting distributions lie reasonably close. The model can thus be considered fully predictive, as it does not require any input for the calculations, other than the distribution of cycle 21 data. The difference between the two results, however, is used for deriving the uncertainty related to its predictive power. Its derivation is discussed in Appendix B.2 where its magnitude can be seen separately (Fig.13). In Fig.6 this systematic effect was included in the model distribution for cycle

³Parentetically, for cycles 21-23 the average duration calculated from sunspots is 10.6 ± 0.7 years, and with the definition using flares it is 11.0 ± 0.8 years.

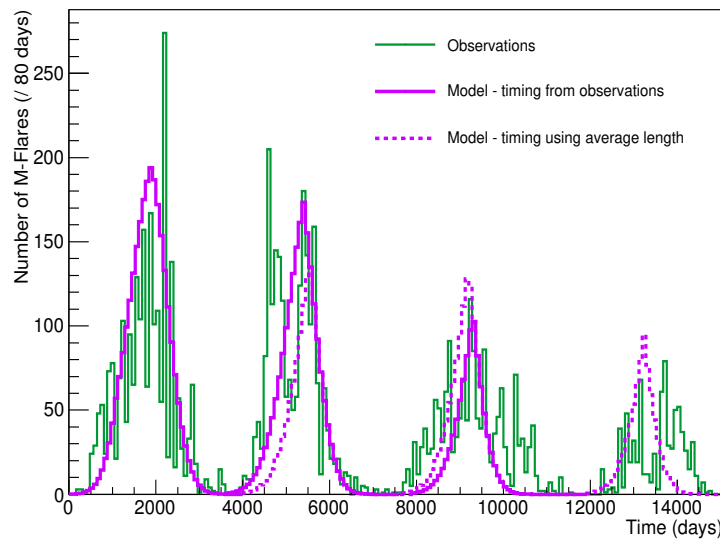


Figure 7: Flare counts for the last four cycles (green), overlaid with model distributions, as obtained by centering the established Gaussians on the measured cycle middles (solid), and on the average cycle length (dotted). (The end of year 2016 is found at day 14,894.)

24.

One could note in addition the possibility that the duration of each cycle is actually related to the time span between consecutive Jupiter-Saturn alignments. However, more cycles would be needed to confirm this. (The first version of the article used this hypothesis for the calculation of the cycles' middles. It is put aside for the time being as it might be “overfitting” on the data.)

2.3 Overview

A quantitative model was presented for the description of the solar cycles in terms of M and X-class flares activity. Although no proposal is made yet about the underlying physical mechanism, the activity was found to be significantly modulated by the relative motion of Jupiter and Saturn. Such an effect could be the manifestation of an internal solar mechanism with an external planetary trigger, however no speculations are made at present about its nature.

More specifically, it is proposed that: *The main drive behind the long-term solar activity is strongly correlated to the approach and retreat of Jupiter and Saturn with respect to their alignments. Every new phase of activity starts as they approach closer than 90° of relative ecliptic longitude. However, this effect can only act within the bounds of the “established” 11-year periodic range.*

We were able to quantify these observations by using two components:

- The combined effect of the two modulations, as quantified by the overlap of two Gaussian functions extracted from the data of cycle 21.
- The determination of individual cycles' temporal middles, provisionally derived from the average sunspot cycle length.

In addition, it is observed that, outside the overlapping area, activity is expected in ranges where both Gaussians still have significant strength, with a decrease towards the date of $+90^\circ$ which separates phases of activity.

The sole input to the model is the temporal distribution of flares in cycle 21 and the date of its middle. Forecasting for other cycles can be done by using the dates of the two planets' alignments. Accordingly, the next Section provides predictions for the rest of cycle 24 and for cycle 25.

Quantification and tests of the model's strength can be found in Appendix A.1. Additional tests in Appendix A.2 probe the possibility that a satisfactory description can emerge randomly from using the specific Gaussian distributions. Both kinds of results provide supplementary support for the proposed mechanism.

3 Forecasting cycles 24 and 25

It is possible to discuss about the evolution of the rest of the current and the next solar cycle, by centering the two types of Gaussians on the appropriate dates over the next years (Fig.8).

As the two planets' alignments move forward with respect to the cycles' middles, two Jupiter-Saturn Gaussians enter the next established Gaussian, a case which our data did not happen to include (but which could actually be settled during cycle 25). However, as discussed in Paragraph 2.1, activity is expected empirically inside all time ranges where both Gaussians have significant strength, so it could be reasonably expected in both overlap regions (i.e. around 17,000 and 19,000 days in Fig.8), probably following the shape of the common area. In any case the cycle's intensity will be lower than that of the current cycle.

The overall picture is compatible with the current "orthodox" expectation of a minimum in solar activity (which is, however, mainly the result of extrapolations from the previous cycles). It should be noted that the prediction will become more accurate upon the start of the next cycle, since the knowledge of the middle of cycle 24 will permit a better centering of the established Gaussian⁴.

⁴The prediction for cycle 25 has changed slightly from the first version of the article, after adopting

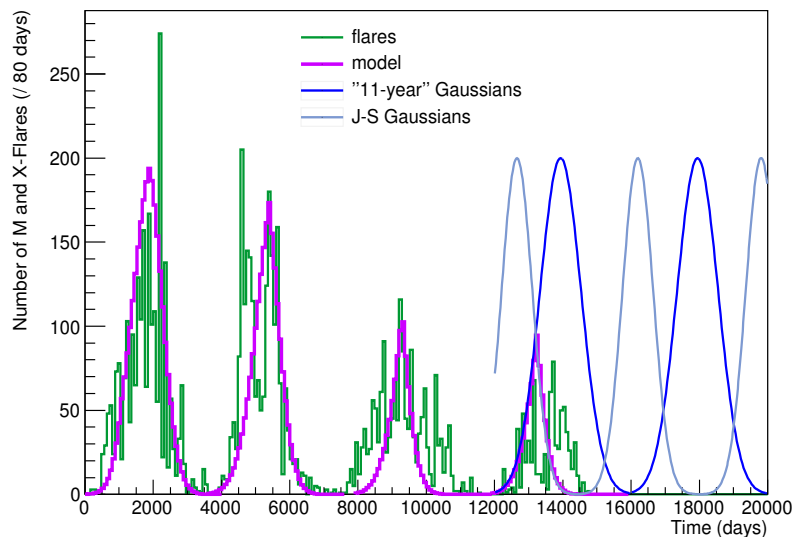


Figure 8: *Flare observations and model distributions, with the two types of Gaussians expanded over the next $\sim 5,000$ days, starting from cycle 24. (The end of year 2016 is found at day 14,894.)*

In between the three overlap ranges no notable activity is expected, but cycle 24 could be characterized by triple peak activity with flares appearing in the first small overlap area. This point could even be settled around the end of year 2017/start of 2018, after some advancement into the first overlap area. Although only measurements up to 2016 were used in the development of the model, flares during 2017 are plotted in the Conclusions (Fig.10).

4 Further discussion

4.1 Other planetary effects

The findings reported in [6], suggesting a relation between short-term evolution of solar activity and the inner planets' positions, can be viewed complementarily with those here. A common description could underlie phenomena of different time scales, with a higher-frequency modulation due to the fast-moving planets closer to the Sun and a more stable long-term element (the solar cycle) due to the massive and slower gas giants.

the centering of the established Gaussians using the average cycle length.

As to planets Uranus and Neptune, although their distance from the Sun makes their contribution appear unlikely, their slow motion can conceivably add a steady underlying element in very-long-scale solar activity. A brief remark can be made about their possible role: During the recorded solar history three conjunctions of Uranus and Neptune took place, in the years 1650, 1821 and 1993. These dates are in the vicinity of the three extrema of recorded activity – the Maunder minimum between years 1650 and 1710, the Dalton minimum in 1800-1820, and the modern maximum in the end of the 20th century – however they obviously include both minima and maxima.

Nonetheless, close to the two minima, the corresponding Jupiter-Saturn alignments occurred at a *normal angle* with respect to that of Uranus and Neptune, while in the case of the maximum Jupiter and Saturn were *aligned* also with Uranus and Neptune. (Notably, just before the Maunder minimum *two* consecutive Jupiter-Saturn alignments actually occurred at a normal angle with respect to the Uranus-Neptune conjunction, conceivably disrupting the formation of two consecutive cycles.)

These concepts remain to be quantified, but a combined effect of this kind is a plausible extension of the mechanism described for Jupiter and Saturn.

4.2 Historical activity

An extrapolation of the model back to the whole era of reliable sunspot records and comparison to sunspot activity could be informative, although there are expected sources of discrepancy: The standard representation of sunspot activity is smoothed to its 13-month mean, the model presented here is not definitive yet on the cases with two Jupiter-Saturn Gaussians entering a single “11-year” Gaussian, and more importantly, a precise correspondence between sunspot and flare activity has not been established in general. Moreover, a complete description should consider all possible planetary effects, as discussed briefly in the previous Paragraph.

At any rate a simplistic extrapolation of the model is shown in Fig.9; dots correspond to the maximum height of the main area of overlap between the two Gaussians in each cycle, and exhibit rough compatibility with the sunspot maxima and general evolution, but displacement in the timing of the minima. More detailed comparison is one goal of the next stage of the analysis.

4.3 On physical mechanisms

Energetic solar events and the solar cycle are widely attributed to a magnetic dynamo mechanism[10] although their modelling is still far from complete[11] and no internal or external regulating factors have been established. Over the past two centuries a number of studies have occasionally pointed out relations between the planets’ periods and solar activity; although planetary tidal effects have been disfavoured[12], other possible explanations have been put forth. However, most of the relevant work is based on

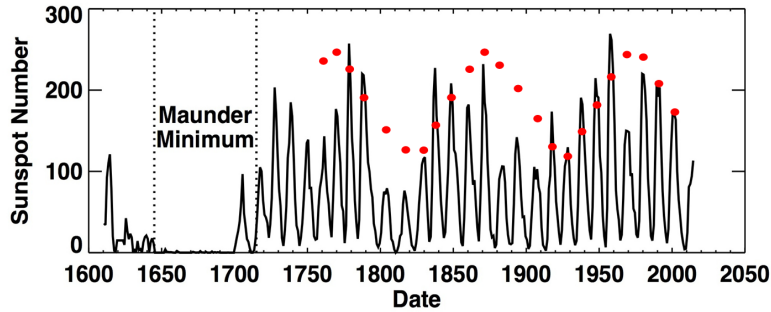


Figure 9: *Extrapolation of the model (red) to the whole era with sunspot records, overlaid with the historical observations (smoothed sunspot monthly averages). The values of the model are normalized to the peak of cycle 23. (Sunspots plot credit: Marshall Space Flight Center/NASA.)*

spectral analysis or pure arithmetic analysis of patterns in solar activity and planetary periods, with only a few studies attempting quantification using timed solar weather events.

We list indicatively some notable recent studies, while pointing out that the discussion is open on several of them. A planetary torque exertion on the tachocline is examined in [13]; the spectral analysis in [14] focusses on the combined effects of Jupiter and Saturn, while [15] focusses on Uranus and Neptune and discusses a spin-orbit coupling mechanism. The latter builds on a proposal based on the motion of the solar system's barycenter [16], which was elaborated recently also in [17] with findings of some similarity to those presented here. It is perhaps noteworthy that all these studies point to a coupling between an internal mechanism and external triggers.

A proposal of different nature is the lensing of dark matter streams[18] in [6], where relation between planetary positions and solar flares was first reported. A recent study with findings similar to [6] concerning the role of the inner planets is presented in [19]. Finally, a remarkable phenomenological study is [20], which directly related planetary positions with terrestrial radio propagation conditions.

At this stage of the present work no inferences are drawn about possible underlying mechanisms. However this modelling, and any further quantification of it, is expected to offer definite hints for their determination.

5 Conclusions

A model was presented for the phenomenological description of long-term solar activity and the quantification of the main features of solar cycles. The principal element of the model is a coupling between the empirical time length of ~ 11 years and the relative ecliptic longitude of the planets Jupiter and Saturn. This coupling was expressed by the

common area of two Gaussian distributions, both extracted from the observations of M and X-class flares in solar cycle 21.

The only other element required is the date of a cycle's temporal middle. Obtaining it from the observations renders the model descriptive for past cycles, while estimating it from the average cycle length is used for predictions.

Thereby, using as input the observations of cycle 21 we reproduce the distributions of activity in the latest three cycles to a satisfactory degree. The model is extended to the next years, providing predictions for the rest of cycle 24 (small third peak) and cycle 25 (weak and "spread-out" in two parts). The component distributions and the resulting model, the observations, the future predictions, as well as observations from year 2017[7] can be seen in Fig.10.

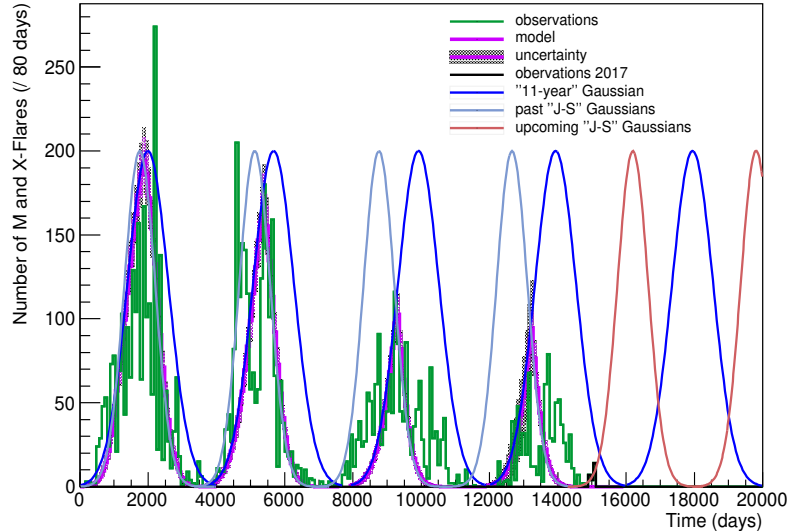


Figure 10: *Overview plot of the model, predictions and data: Flare counts for the last four cycles, overlaid with the model distributions including statistical and systematic uncertainty. The two types of Gaussians contributing to the model are also shown and projected over the next years. Flare counts from the year 2017 up to 6th September have been added.*

This model describes mainly the central part of the cycles, with phenomenological remarks about the outer ranges remaining to be quantified in subsequent steps of the analysis. Other planned optimizations include use of the flares' intensity and position.

Although no proposal is made about the underlying physical mechanism, these results point strongly to a correlation between the triggering of solar activity and the relevant position of the gas giants, with the activity increasing and declining respectively with their approach and retreat. While numerical relations between the time lengths involved in these effects have been noticed in the past, they were not quantified by using actual solar events. The present results and further quantification are expected to contribute

to the understanding of the mechanisms involved in solar dynamics, and they could be employed in long-term forecasting of space weather.

Acknowledgments

The author is indebted to Juan-Carlos Algaba, Jonghee Yoo, Kalliopi Iordanidou and Jonathan Elkin for the useful discussions, and particularly to Konstantin Zioutas.

Provision of solar X-ray flux measurements by the USA National Oceanic and Atmospheric Administration and sunspots data by the Royal Observatory of Belgium is acknowledged.

Part of this work was supported by grant IBS-R017-D1-2017-a00 of the Republic of Korea.

References

- [1] D.H. Hathaway, R.M. Wilson, E.J. Reichmann, “The shape of the sunspot cycle”. *Sol. Phys.* 151, 177 (1994)
- [2] D.H. Hathaway, R.M. Wilson, E.J. Reichmann, “A synthesis of solar cycle prediction techniques”. *J. Geophys. Res.* 104, 22,375 (1999)
- [3] NOAA Space Weather Prediction Center. Solar Cycle 24 Prediction Updated May 2009. <http://www.swpc.noaa.gov/content/solar-cycle-24-prediction-updated-may-2009> (2009)
- [4] D.H. Hathaway, R.M. Wilson, “Geomagnetic activity indicates large amplitude for sunspot cycle 24”. *Geophys. Res. Lett.* 33, 18101 (2006)
- [5] D.H. Hathaway, “The Solar Cycle”. *Living Reviews in Solar Physics* 12, 4 (2015)
- [6] S. Bertolucci, K. Zioutas, S. Hofmann, M. Maroudas, “The Sun and its Planets as detectors for invisible matter”. *arXiv:1602.03666* (2016)
- [7] Archives of the Space Weather Prediction Center and the National Centers for Environmental Information, USA National Oceanic and Atmospheric Administration. <http://www.swpc.noaa.gov>, <https://www.ngdc.noaa.gov>
- [8] Archive of the Solar Influences Data Analysis Center, Royal Observatory of Belgium. <http://www.sidc.be/silso>
- [9] R. Brun, F. Rademakers, “ROOT - An Object Oriented Data Analysis Framework”. *Nucl. Inst. & Meth. in Phys. Res.* A389, 81 (1997)

- [10] E.N.Parker, “Hydromagnetic dynamo models”. *Astrophys. J.* 122, 293 (1955)
- [11] For instance: H.C.Spruit, “Theories of the solar cycle: a critical view”, *arXiv:1004.4545* (2010)
- [12] C.M.Smythe, J.A.Eddy, “Planetary tides during the Maunder Sunspot Minimum”. *Nature* 266, 434 (1977)
- [13] J.A.Abreu et al, “Is there a planetary influence on solar activity?”. *A&A* 548, A88 (2012)
- [14] N.Scafetta, “Multi-scale harmonic model for solar and climate cyclical variation throughout the Holocene based on Jupiter–Saturn tidal frequencies plus the 11-year solar dynamo cycle”. *JASTP* 80, 296 (2012)
- [15] G.J.Sharp, “Are Uranus & Neptune Responsible for Solar Grand Minima and Solar Cycle Modulation?”. *IJAA* 3, 260 (2013)
- [16] P.D.Jose, “Sun’s Motion and Sunspots”. *Astrophys. J.* 70, 193 (1965)
- [17] I.R.G.Wilson, B.D.Carter, I.A.Waite, “Does a spin-orbit coupling between the Sun and the Jovian planets govern the solar cycle?”. *Pub. of the Astr. Soc. of Australia* 25, 85 (2008)
- [18] K.Freese, P.Gondolo, H.J.Newberg, “Detectability of weakly interacting Massive Particles in the Sagittarius dwarf tidal stream”. *Phys. Rev. D* 71, 043516 (2005)
- [19] I.Edmonds, “Revisiting 154-day periodicity in the occurrence of hard flares. A planetary influence?”. *arXiv:1611.04240* (2016)
- [20] J.H.Nelson, “Shortwave radio propagation correlation with planetary positions”. *RCA Review*, XII, 1 (1951)

A Performance and statistical testing

The performance of the model on some of the main features of the cycles and its correlation with the data are examined in Paragraph A.1 (similar tests appear in [2] for existing models). In Paragraph A.2 it is tested whether a satisfactory agreement between the data and the overlapping of the two used Gaussians could arise randomly, or if it is indeed related to the two planets’ synodic period.

A.1 Performance

The performance of the model is tested by using the quantities listed below for describing some of the cycles’ main features in more specific terms. All comparison is between the observations and the distributions from the model. The bin with the global maximum in cycle 21 is excluded from all calculations in Paragraph A.1 as an outlier. “Maximum count” will refer to the largest bin content within a specified range.

- Difference in maximum count within the range 0° - 45° ⁵ (measured in counts and in standard deviations).
- Distance of the positions of the maximum count within 0° - 45° (in bins).
- Difference in global maximum count (in counts and in deviations).
- Distance of the positions of the cycles’ start, as defined by the first bin with $\geq 5\%$ of the maximum data count within 0° - 45° (in bins).

The values of these quantities are given in Table 3. The standard deviation is calculated from the statistical uncertainty and all applicable sources of systematics (Appendices B.1, B.2). As described in Paragraph 2.2, the cycles’ middles are either known from the observations (cycles 21, 22, 23) or estimated from the average cycle length (cycles 22, 23, 24); the aggregated result for the second case is also quoted.

In addition, the Pearson correlation coefficient between the distributions of flares from observations and from the model has the values 0.88 and 0.73, within 0° - 45° and in the whole range respectively (Fig.11). (The exclusion of bins empty in both data and model shifts the values by 0.01.) In both cases the p-value for this correlation arising by chance is smaller than 10^{-7} , as calculated from random permutation of the two sets of datapoints. When the cycles’ middles are estimated from the average cycle length, the values become 0.85 and 0.73.

A.2 Timing

It will be tested whether a satisfactory agreement between the data and the overlapping of the two used Gaussians (Table 2) could arise randomly, or if it is indeed connected to the two planets’ synodic period (Paragraph 2.1). For this, the periodic displacement between the two Gaussians is let to vary arbitrarily, and the agreement between the resulting predictions and the data is checked: To do so, while the actual average length between consecutive alignments is 3,634 days, its value is let to iterate between 2,000 and 5,000 days. Then the Kolmogorov-Smirnov test is applied (with the ROOT[9] package),

⁵The range 0° - 45° , the “central part” of the cycles, is described more accurately by the model by construction.

Table 3: Values for quantifiers of some of the cycles’ main features, for each cycle and for their RMS. The numbers are the absolute difference between the predictions and the data. Each bin of the two distributions spans 80 days. The last column (shaded) gives the RMS when using the average cycle length for centering the established Gaussians.

	C 21	C 22	C 23	C 24	RMS	RMS av. length
Difference in max* in 0° - 45° (in counts [and in σ s])	27 [1.35]	7 [0.38]	14 [1.10]	26 [0.92]	20.3 [1.00]	29.9 [1.26]
Distance between max in 0° - 45° (in bins)	0	0	1	2	1.1	1.5
Difference in global max (in counts [and in σ s])	27 [1.35]	32 [1.74]	14 [1.10]	15 [0.53]	23.3 [1.26]	41.9 [1.76]
Distance between start of cycle [†] (in bins)	2	3	8	1	4.4	4.4

* “Max” refers to the maximum count. † See text for definition.

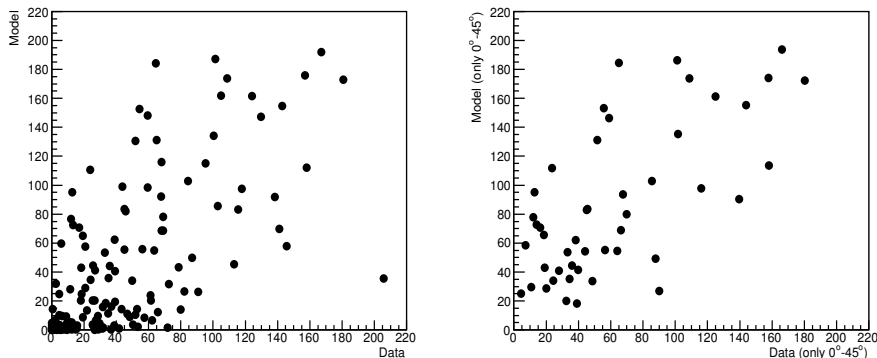


Figure 11: Distribution of counts of flares in the model versus observations. Left: For the whole time range; 184 points. Right: Within the range 0° - 45° of each cycle; 47 points.

to check the compatibility of the data with the predicted distributions for each value of the time length.

Although including the dataset used for the derivation of the model should be avoided in the Kolmogorov-Smirnov test, it is assumed that in the present case the model was derived too indirectly from the distribution of cycle 21 (Paragraph 2.1), therefore it is appropriate to include all cycles in the test. Ideally, the test should be performed on unbinned data. For this, we perform the test both with the binning used in the rest of the analysis (80 days per bin) and with one bin per day. (In principle this introduces a source of uncertainty because of the need to change the constant of the Gaussians to match the new histogram’s scale; however, the results from the two runs are almost identical, so this uncertainty was not incorporated in the calculations.)

As seen in Fig.12, the tests with the two binnings show a well-defined global minimum at 3,740 days, i.e. 2.9% away from the actual value for the average length between alignments (3,634), while at the same time no similarly strong minima occur for other lengths. Overall, the test supports the non-randomness of the proposed mechanism.

Finally, it can be noted that the chi-square test cannot be used here because of the many predicted empty bins and their importance. Still, ad hoc modifications on it for evading the empty bins result in similarly well-defined minima, in proximity to the actual value of the average length between alignments.

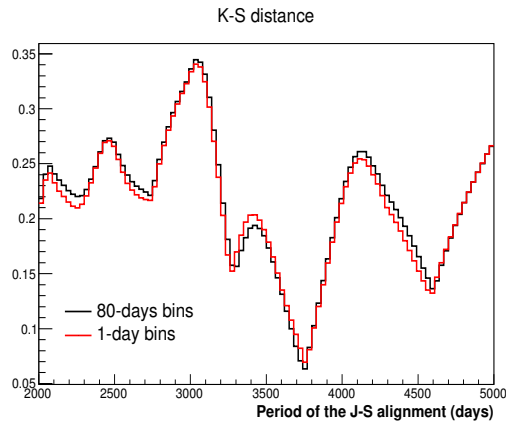


Figure 12: *Kolmogorov-Smirnov distances for varying numbers of the time length between alignments, for data binned in 80 days (black) and with one bin per day (red).*

B Systematic uncertainties

B.1 Binning effects

Different binning choices change the short-scale distribution of flares in each cycle, a fact which should be reflected in the model's degree of goodness. There are two sources of uncertainty: The bin size, and the position of the start date of data within the first bin. In both cases, re-deriving the two Gaussians for different choices would add complication, since the fit used quasi-empirical constraints (Paragraph 2.1). Instead, we plot again the observed number of flares in cycle 21 while varying (i) the number of bins by ± 6 around the original number 50, in steps of 2; and separately (ii) the position of the start date by 0 to 70 days, in steps of 10. Then we calculate the chi-square over the number of degrees of freedom between the original prediction and each resulting data distribution. And we use the standard deviation from all instances for the uncertainty value in each of the two cases. Only the bins between around $\pm 1,500$ days were used, for stability and to avoid empty bins.

The resulting uncertainty is 7.4% on the original χ^2/ndof from the bin size and 6.1% from the start date. The two uncertainties are not added, but rather considered as a measure of the change incurred by binning choices in general. The larger value, 7.4% is kept and applied to each bin of the model in all cycles (as seen in Fig.6).

B.2 Average cycle length

As described in Paragraph 2.2, the “11-year” Gaussian is centered on one average sunspot cycle length away from the last measured cycle middle. As seen from cycles 22 and 23 (Fig.7), this estimation results in significant systematic uncertainty, although the available dataset is too small for its reliable calculation. In any case, the following steps were taken for its estimation.

In cycles 22/23 the calculated date when using the average length falls +343/-222 days away from the actual middle. The average of these two numbers’ absolute value, 282, was used. With only two datapoints available, the resulting uncertainty will probably be overestimated; therefore, only half of 282 is considered, as an ad hoc approximation.

As described in Paragraph 2.1, the model is constructed by selecting the lower value among the two Gaussians in each bin. Accordingly, the uncertainty is found by centering the established Gaussian at ± 141 days around its originally projected date for each cycle and obtaining the model distribution. The results are shown in Fig.13. They are applicable whenever the average cycle length is used for the timing of the established Gaussian.

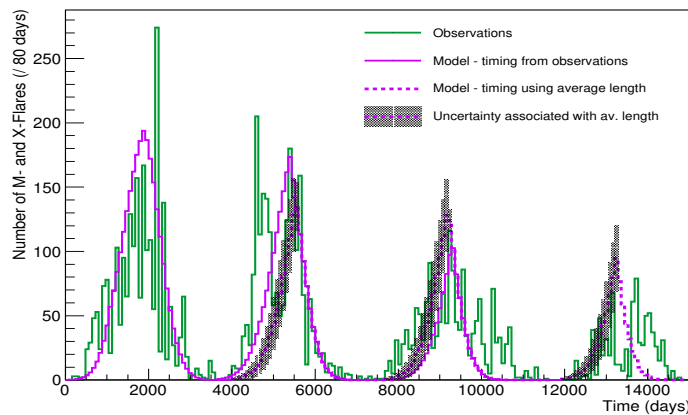


Figure 13: Flare counts for the last four cycles (green), overlaid with model distributions, as obtained by centering the established Gaussians on the measured cycle middles (solid), and on the average cycle length (dotted). The systematic uncertainty due to the centering of the established contribution is shown as shade around the dotted line.